RSC Advances

PAPER

View Article Online
View Journal | View Issue

Cite this: *RSC Adv.*, 2023, **13**, 18496

Anti-Alzheimer activity of new coumarin-based derivatives targeting acetylcholinesterase inhibition†

Nahla N. Kamel,[a] Hanan F. Aly,*[a] Ghadha I. Fouad,[a] Somaia S. Abd El-Karim,[a] Manal M. Anwar,[a] Yasmin M. Syam,[a] Samia A. Elseginy,[b] Kawkab A. Ahmed,[c] Hoda F. Booles,[d] Mohamed B. Shalaby,[e] Wagdy K. B. Khalil,[d] Rajat Sandhir,[f] Sonam Deshwal[f] and Maha Z. Rizk[a]

New 2-oxo-chromene-7-oxymethylene acetohydrazide derivatives **4a–d** were designed and synthesized with a variety of bioactive chemical fragments. The newly synthesized compounds were evaluated as acetylcholinesterase (AChE) inhibitors and antioxidant agents in comparison to donepezil and ascorbic acid, respectively. Compound **4c** exhibited a promising inhibitory impact with an IC_{50} value of 0.802 μM and DPPH scavenging activity of 57.14 ± 2.77%. Furthermore, biochemical and haematological studies revealed that compound **4c** had no effect on the blood profile, hepatic enzyme levels (AST, ALT, and ALP), or total urea in **4c**-treated rats compared to the controls. Moreover, the histopathological studies of **4c**-treated rats revealed the normal architecture of the hepatic lobules and renal parenchyma, as well as no histopathological damage in the examined hepatic, kidney, heart, and brain tissues. In addition, an *in vivo* study investigated the amelioration in the cognitive function of AD-rats treated with **4c** through the T-maze and beam balance behavioural tests. Also, **4c** detectably ameliorated MDA and GSH, reaching 90.64 and 27.17%, respectively, in comparison to the standard drug (90.64% and 35.03% for MDA and GSH, respectively). The molecular docking study exhibited a good fitting of compound **4c** in the active site of the AChE enzyme and a promising safety profile. Compound **4c** exhibited a promising anti-Alzheimer's disease efficiency compared to the standard drug donepezil.

Received 9th April 2023
Accepted 29th May 2023

DOI: 10.1039/d3ra02344c

rsc.li/rsc-advances

1. Introduction

Alzheimer's disease (AD) is one of the most common forms of dementia occurring in the elderly population worldwide, and is the most common fatal age-related neurodegenerative disease, characterized by a decline of cholinergic function, progressive loss of brain function, and memory decline. Approximately 13% of people over the age of 65 and 45% of people over the age of 85 are estimated to have AD.[1] According to mounting evidence from genetic, pathological, and functional studies, there is an imbalance between the production and clearance of amyloid β (Aβ) peptides in the brain, resulting in their accumulation and aggregation. The toxic Aβ aggregates in the form of soluble Aβ oligomers, intraneuronal Aβ, and amyloid plaques injure synapses and ultimately cause neurodegeneration and dementia.[2] The toxicity of Aβ seems to depend on the presence of the microtubule-associated protein tau, the hyper-phosphorylated forms of which aggregate and deposit in AD brains as neurofibrillary tangles and prevent the passage of essential molecules and nutrients.[3] This causes axonal transport dysfunction and neuronal loss.[4] Moreover, theories such as the neurotoxicity of the excitatory neurotransmitters, altered insulin signaling, oxidative stress, and inflammation can also explain the causes of dementia and provide a new theoretical basis and therapeutic target for the development of novel drugs for AD.[5] Acetylcholine esterase (AChE) is the most vital enzyme that maintains the balance of acetylcholine levels. Many studies have suggested a relationship between learning and memory functions and AChE activity in experimental animals.[6] Thus, the use of acetylcholinesterase (AChE) inhibitors like rivastigmine or dopenzil that increase the availability of acetylcholine at cholinergic synapses represents a major therapeutic approach

[a]*Department of Therapeutic Chemistry, National Research Centre, 12262 El-Bohouth St, Cairo, Egypt. E-mail: Hanan_abduallah@yahoo.com*
[b]*Green Chemistry Department, Chemical Industries Research Division, National Research Centre, P. O. Box 12622, Egypt*
[c]*Pathology Departments, Faculty of Veterinary Medicine, Cairo University, Giza, 12211, Egypt*
[d]*Department of Cell Biology, National Research Centre, 12262 El-Bohouth St, Cairo, Egypt*
[e]*Toxicology Research Department, Research Institute of Medical Entomology (RIME), General Organization of Teaching Hospitals and Institutes (GOTHI), Ministry of Health and Population (MoHP), Dokki, P. O. Box 12311, Cairo, Egypt*
[f]*Department of Biochemistry, Panjab University, Chandigarh, India*

† Electronic supplementary information (ESI) available. See DOI: https://doi.org/10.1039/d3ra02344c

to the disease.[7] Literature survey showed that the coumarin nucleus, also known as 2*H*-1-benzopyran-2-one constitutes the main structural component of many natural products and synthetic compounds with a wide range of biological activity. Coumarins are intriguing compounds for drug discovery in the arena of AChEIs because of the possibility of chemical substitutions at numerous places in this core structure.[8] The coumarin moiety's potential to inhibit cholinesterase enzymes has been demonstrated in recent *in vitro* assays. Furthermore, the coumarin nucleus has a number of biological effects on various aspects of Alzheimer's disease, in addition to AChE suppression, including inhibition of the enzyme secretase-1 (BACE-1), cyclooxygenase (COX)/lipoxygenase (LOX) antagonists, antagonists of the cannabinoid receptor 2 (CB2), agonists of the gamma amino butyric acid (GABA) receptor, antagonists of the NMDA receptor, and monoamineoxidase (MAO) inhibitors.[9–12] Many coumarin natural products are have anti-Alzheimer activity, such as esculetin **I**, decursinol **II**, scopoletin **III**, and mesuagenin **IV**.[13]

Docking studies using 2*H*-chromen-2-one demonstrate this nucleus's ability to attach to the peripheral anionic sites (PAS) of both isoforms of cholinesterase, simulating the enzyme's natural substrate. Because of this value, medicinal chemists working on medicines for AD have viewed coumarin as a preferred scaffold for combining with other pharmacophores that can interact with different targets.[14] It has been investigated that the use of benzyloxy group at position 7 of the coumarin scaffold has a significant impact on AChE inhibitory activity, as seen in compounds **V**, **VI**,[15] and **VII**.[16] In addition, AChE inhibitory activity may have increased as a result of the 4-fluorophenyl ring forming π–π stacking with Trp86, as revealed by a closer investigation of compound **VII**'s binding mechanism.[16] Additionally, studies showed that the coumarin's substitution at position 4 emphasizes its AChE inhibitory activity, which is found in compounds **VIII**,[17] and **IX**[18] (Fig. 1).

Moreover, different studies exhibited that numerous AChEIs have various aromatic or heterocylic rings conjugated with coumarin cores *via* nitrogenous linkers, which were intended to stabilize the molecules within the gorge of the AChE enzyme.[19] Thus, it was thought valuable to present new compounds as promising potent AChEIs, having the coumarin scaffold conjugated with different distinct aromatic and/or heterocycles at position 7 *via* an appropriate oxyacetohydrazide linker, in order to gain new compounds with potent AChE inhibitory activity and a safe profile for AD treatment (Fig. 2).

Based on molecular docking study as acetylcholinesterase inhibitors, the target compounds were selected and synthesized. The biosafety of the new compounds was also determined. Furthermore, the inhibitory activity of the most active compound as well as its impact on several biomarkers related to

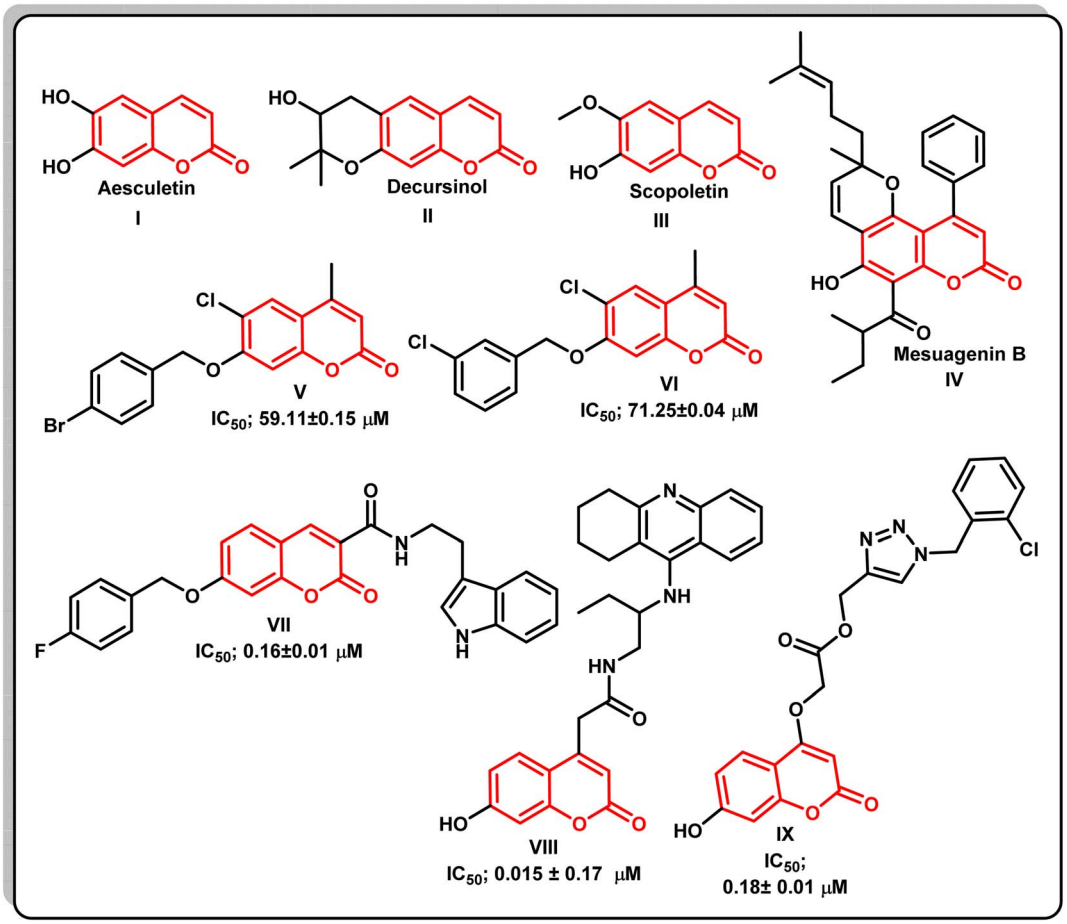

Fig. 1 The chemical structures of various naturally occurring and synthetic coumarin compounds with AChE inhibitory activity.

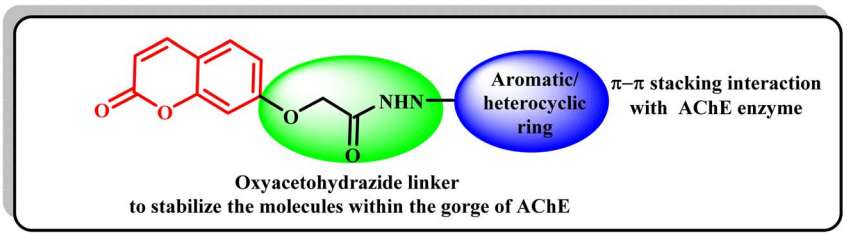

Fig. 2 The strategy of the development of new coumarin compounds as AChE inhibitors.

the disease were investigated. In addition, the impact of the most promising compound on the amelioration of the disorders associated with these biomarkers in AD was elucidated. Molecular docking study was carried out to find out the binding mode of the most active compound to interact with the active site of the target enzyme.

2. Experimental

2.1. Chemical synthesis

The instruments used to determine melting points, spectral data (IR, ^{1}H NMR, ^{13}C NMR, and mass), as well as chemical analyses were included in a detailed description of the in ESI file.†

2.1.1. Synthesis of ethyl-2-((4-methyl-2-oxo-2*H*-chromen-7-yl)oxy)acetate (2). A mixture of 7-hydroxy-4-methyl-2*H*-chromen-2-one (**1**) (1.7 g; 10 mmol) in acetone (30 mL) was refluxed with ethyl bromoacetate (10 mmol) and K_2CO_3 (1.38 g) for 12 h. After cooling, the organic solvent was concentrated and the obtained solid was filtered washed several times with water, dried, and crystalized from ethanol to give the compound **2**.[20]

2.1.2. Synthesis of 2-((4-methyl-2-oxo-2*H*-chromen-7-yl)oxy) acetohydrazide (3). A solution of compound **2** (2.60 g; 10 mmol) in ethanol (25 mL) was refluxed with hydrazine hydrate (0.75 mL, 15 mmol) for 3 h. After concentrating the reaction mixture, the solid mass obtained was filtered and recrystallized from ethanol to give compound **3**.[20]

2.1.3. Synthesis of 2-((4-methyl-2-oxo-2*H*-chromen-7-yl) oxy)-*N*′-substituted (methylene)acetohydrazide derivatives 4a–d. A solution of compound **3** (0.50 g, 2 mmol) and various aromatic ketones and aldehydes, including α-tetralone, isatin, 1-indanone, and 4-carboxybenzaldehyde (2 mmol) in ethanol (25 mL) was refluxed for 2–3 h. After cooling to room temperature, the separated solid mass was filtered, and recrystallized from ethanol to give the target derivatives **4a–d**.

*2.1.3.1. N′-(3,4-dihydronaphthalen-1(2H)-ylidene)-2-((4-methyl-2-oxo-2H-chromen-7-yl)oxy)acetohydrazide (**4a**).* White solid, yield 78.0%; IR (KBr, cm^{-1}): 3354 (NH), 1720, 1660 (2C=O), 3056 (aromatic C–H), and 2914.5 (alkane C–H); ^{1}H NMR (500 MHz, DMSO-d$_6$): δ 1.82, 2.63, 2.73 (3m, 6H, 3CH$_2$-tetralone ring), 2.39 (s, 3H, CH$_3$), 4.90 (s, 2H, OCH$_2$ minor conformer), 5.35 (s, 2H, OCH$_2$ major conformer), 6.21 (s, 1H, coumarin-H$_3$), 6.94–7.03 (m, 2H, Ar–H), 7.19–7.29 (m, 3H, Ar–H), 7.67–7.71 (m, 1H, Ar–H), 8.08 (dd, 1H, Ar–H, J = 7.5 Hz), 10.62 (br, 1H, NH, minor conformer, D$_2$O exchangeable), 10.90 (br, 1H, NH, major conformer, D$_2$O exchangeable); ^{13}C NMR (125 MHz, DMSO-d$_6$): δ 18.53 (CH$_3$), 21.71, 25.85, 29.29 (3CH$_2$-tetralone ring), 66.08 (–OCH$_2$), 101.98, 111.62, 112.78, 113.74, 124.99, 126.71, 126.77, 128.93, 129.51, 132.51, 140.27, 148.86, 153.75, 155.00, 160.53, 161.88 (CO), 169.63 (C=O); anal. calcd for: C$_{22}$H$_{20}$N$_2$O$_4$: C, 70.20; H, 5.36; N, 7.44, found: C, 70.52; H, 5.06; N, 7.15.

*2.1.3.2. 2-((4-Methyl-2-oxo-2H-chromen-7-yl)oxy)-N′-(2-oxoindolin-3-ylidene) acetohydrazide (**4b**).* White solid, yield 67.0%; IR (KBr, cm^{-1}); 3355 (NH), 1720.5, 1695, 1660 (3C=O), 3062 (aromatic C–H), and 2920 (alkane C–H); ^{1}H NMR (500 MHz, DMSO-d$_6$): δ 2.40 (s, 3H, CH$_3$), 5.01 (s, 2H, OCH$_2$, major conformer), 5.45 (s, 2H, OCH$_2$, minor conformer), 6.25 (s, 1H, coumarin-H$_3$), 6.96 (d, 1H, Ar–H, J = 7.5 Hz), 7.09–7.10 (m, 3H, Ar–H), 7.39 (t, 1H, Ar–H, J = 7.5 Hz), 7.56 (br, 1H, Ar–H), 7.75 (br, 1H, Ar–H), 11.29 (s, 1H, NH, D$_2$O exchangeable), 12.58 (br, 1H, NH, minor conformer, D$_2$O exchangeable), 13.70 (s, 1H, NH, major conformer, D$_2$O exchangeable); ^{13}C NMR (125 MHz, DMSO-d$_6$): δ 18.53 (CH$_3$), 66.54 (–OCH$_2$), 102.78, 111.63, 112.16, 112.84, 120.04, 121.45, 123.08, 127.05, 132.35, 143.08, 153.66, 154.99, 160.40, 162.97 (CO), 167.00 (C=O); anal. calcd for: C$_{20}$H$_{15}$N$_3$O$_5$: C, 63.66; H, 4.01; N, 11.14; found: C, 63.46; H, 4.31; N, 11.54.

*2.1.3.3. N′-(2,3-Dihydro-1H-inden-1-ylidene)-2-((4-methyl-2-oxo-2H-chromen-7-yl)oxy)acetohydrazide (**4c**).* White solid, yield 77.0%; IR (KBr, cm^{-1}); 3340 (NH), 1715, 1660 (2C=O), 3057 (aromatic C–H), and 2920 (alkane C–H); ^{1}H NMR (500 MHz, DMSO-d$_6$): δ 2.39 (s, 3H, CH$_3$), 2.80–2.87 (m, 2H, CH$_2$ indane ring), 3.07–3.09 (m, 2H, CH$_2$, indane ring), 4.88 (s, 2H, OCH$_2$, minor conformer), 5.30 (s, 2H, OCH$_2$, major conformer), 6.22 (s, 1H, coumarin-H$_3$), 6.94–7.04 (m, 2H, Ar–H), 7.30–7.41 (m, 3H, Ar–H), 7.65–7.73 (m, 2H, Ar–H), 10.49 (s, 1H, NH, minor conformer, D$_2$O exchangeable), 10.82 (s, 1H, NH, major conformer, D$_2$O exchangeable); ^{13}C NMR (125 MHz, DMSO-d$_6$): δ 18.55 (CH$_3$), 27.48, 28.55 (2CH$_2$, indane ring), 65.87 (–OCH$_2$), 101.97, 111.64, 112.76, 112.84, 121.75, 126.13, 126.82, 127.37, 127.50, 130.97, 137.98, 153.79, 155.02, 158.61, 160.55, 161.91 (C=O), 169.21 (C=O); anal. calcd for: C$_{21}$H$_{18}$N$_2$O$_4$: C, 69.60; H, 5.01; N, 7.73; found: C, 69.21; H, 5.41; N, 7.52.

*2.1.3.4. 4-((2-(2-((4-Methyl-2-oxo-2H-chromen-7-yl)oxy)acetyl) hydrazineylidene)methyl) benzoic acid (**4d**).* White solid, yield 75.0%; IR (KBr, cm^{-1}); 3445 (OH), 3360 (NH), 1710, 1695, 1665 (3C=O), 3054 (aromatic C–H), and 2920 (alkane C–H); ^{1}H NMR (500 MHz, DMSO-d$_6$): δ 2.39 (s, 3H, CH$_3$), 4.84 (s, 2H, OCH$_2$, minor conformer), 5.33 (s, 2H, OCH$_2$, major conformer), 6.21 (s, 1H, coumarin-H$_3$, major conformer), 6.24 (s, 1H, coumarin-H$_3$, minor conformer), 6.99–7.06 (m, 2H, Ar–H), 7.69 (d, 1H, Ar–H, J = 8.5 Hz, major conformer), 7.73 (d, 1H, Ar–H, J = 8.5 Hz, minor

conformer), 7.82 (d, 2H, Ar–H, J = 8.5 Hz, minor conformer), 7.85 (d, 2H, Ar–H, J = 8.5 Hz, major conformer), 7.97–8.00 (m, 2H, Ar–H), 8.07 (s, 1H, –N=CH, major conformer), 8.38 (s, 1H, –N=CH, minor conformer), 11.82 (s, 1H, NH, D_2O exchangeable, minor conformer), 11.83 (s, 1H, NH, D_2O exchangeable, major conformer); 12.63 (br, H, COOH, D_2O exchangeable); ^{13}C NMR (125 MHz, DMSO-d_6): δ 18.54 (CH_3), 65.70 (–OCH_2), 102.05, 111.68, 112.83, 113.82, 126.79, 127.00, 127.45, 127.62, 130.12, 132.11, 138.39, 143.38, 153.76, 155.03, 160.54, 161.79 (CO), 167.32 (C=O), 169.10 (C=O); anal. calcd for: $C_{20}H_{16}N_2O_6$: C, 63.16; H, 4.24; N, 7.37.

2.2. Biological evaluation

2.2.1. *In vitro* studies

2.2.1.1. Acetylcholinesterase inhibition screening protocol. Acetylcholinesterase (AChE) inhibitory activity was measured using quantitative colorimetric assay according to the method developed by Ellman *et al.*[21] More details are in the ESI file.†

2.2.1.2. Antioxidant assay by DPPH. In vitro estimation of antioxidant activity according to Gulcin *et al.*[22]

2.2.1.2.1. Calculation. Inhibition (%) = read of control − read of test/read of control × 100.

2.2.2. *In vivo* studies

2.2.2.1. Animal care. Wistar albino rats weighing between 180–200 g were housed in the animal house of National Research Centre. More details are in the ESI file.†

2.2.2.2. Biosafety assay. Different concentrations of the most promising synthetic compounds were used to determine LD_{50} in experimental animals for 24 hours. LD_{50} is the dose that produces mortality in 50% of animals. For each concentration six animals were used.

2.2.2.3. Toxicity study. Selected 8 Wistar rats of uniform weight were taken and divided into two groups of 4 rats each for each concentration. The synthesized compound **4c** was given orally to rats in doses 50 and 100 mg per kg b.wt as described by Desoukey *et al.*[23] More details are in the ESI file.†

2.2.2.3.1. Acute toxicity. No mortality was observed at the dose of 50 mg per kg b.wt. While, one rat of 4 in the group administered 100 mg per kg b.wt died post 24 h (25%). No further death or any behaviour changes were observed for one month. Thus, the applied dose for the compound **4c** was considered to be (10 mg per kg b.wt), which is the dose applied for the reference drug donepezil.

2.2.2.3.2. Chronic toxicity. In chronic toxicity, we used 1/10 of the LD_{50} (10 mg per kg b.wt) supplemented orally to male Wistar rats for one month and didn't see any indication of harmfulness (no mortality, no going bald, no loose bowels, and so on). Moreover, irregularities in conduct, food and water admissions, and well-being status among the treated creatures weren't noticed. Toxicity tests on liver and kidney functions, as well as a complete blood picture, were also performed.

2.2.2.4. Histopathological investigation. Specimens of liver, kidneys, heart, and brain were harvested from all mice/group, immediately fixed in 10% neutral buffered formalin, and routinely processed according to Suvarna *et al.*[24] Sections of 4–5 μm thickness were prepared and stained with Hematoxylin and Eosin (H&E), for histopathological examination by a light microscope (Olympus BX50, Tokyo, Japan).

2.2.2.5. Biochemical analyses

2.2.2.5.1. In vivo studies. After one month, rats were anaesthetized with diethyl ether, blood was drawn *via* sublingual vein rupture, and rats were decapitated. Blood samples were centrifuged at 3000 rpm, and the clear serum that was separated was frozen at −80 °C for biochemical analysis.[25–29] More details are in the ESI file.†

2.2.2.5.2. Induction of $AlCl_3$ and grouping of animals. Induction of $AlCl_3$-induced Alzheimer's disease. $AlCl_3$ solutions were made freshly at the beginning of each experiment. $AlCl_3$ was dissolved in drinking water and administered orally to rats daily for two months at 0.5 mL per 100 g b.wt at a dose of 100 mg kg^{-1}.[30]

2.2.2.5.3. Behaviour studies. The neurocognitive function of rats was estimated by T-maze test (constructed in the NRC, Egypt) according to Deacon and Rawlins.[31] Before performing this experiment, the animals were left without food for 24 h, with only water to drink.[32,33] More details are in the ESI file.†

2.2.2.6. In vivo determination of oxidative stress

2.2.2.6.1. Blood sample preparation. The rats were fasted overnight. Then, they were anaesthetized by inhaling 1.9% diethyl ether on a small piece of cotton (0.08 mL per litre of container volume). Blood samples were collected after anaesthetizing the animals using a cardiac puncture in a clean and dry test tube. Blood was left to clot for 10 minutes and centrifuged at 3000 rpm (1.1750*g*) to obtain serum. The separated serum was stored at −80 °C for biochemical analyses.

2.2.2.6.2. Brain tissue sampling preparation. At the end of the experiment, the rats were fasted overnight, subjected to anaesthesia, and scarified. The whole brain of each rat was rapidly dissected, washed with isotonic saline, and dried on filter paper.[34,35] More details are in the ESI file.†

2.3. Molecular docking studies

The crystal structure of acetylcholinesterase (PDB: 1EVE) was retrieved from Protein Data Bank (**http://www.rcsb.org**). Protein is prepared with Molecular Operating Environment (MOE) software; the water was removed, and the hydrogen atoms were added using MOE. More details are in the ESI file.†

3. Results and discussion

3.1. Chemistry

A new series of 2-((4-methyl-2-oxo-2*H*-chromen-7-yl)oxy)-*N*′-substituted (methylene)acetohydrazide derivatives **4a–d** were synthesized according to the synthetic route adopted in Scheme 1. The key starting compound 7-hydroxy-4-methyl-2*H*-chromen-2-one (**1**) was refluxed with ethyl bromoacetate in the presence of anhydrous potassium carbonate in acetone to give the corresponding ester **2**. Hydrazinolysis of compound **2** with hydrazine hydrate produced the corresponding acetohydrazide **3** in a good yield.[20] Furthermore, condensation of compound **3** with

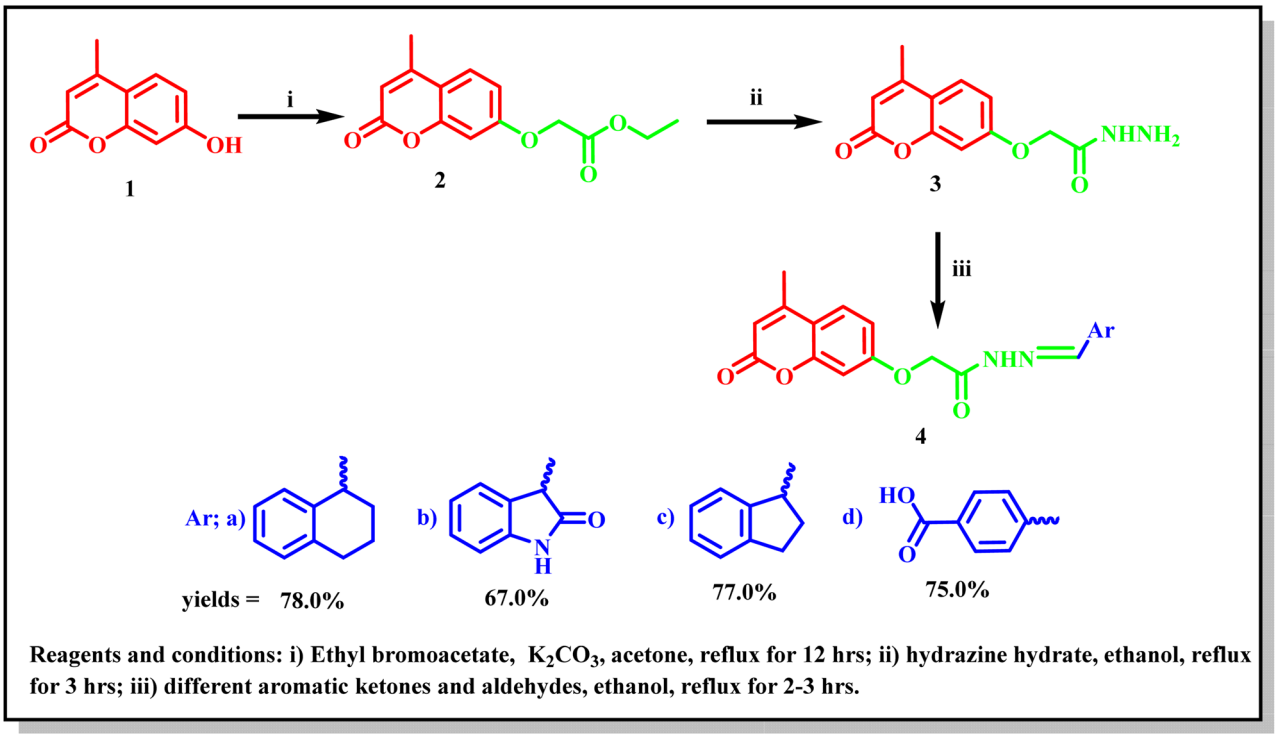

Scheme 1 Synthetic route for the synthesis of the target 4-methyl-2-oxo-2*H*-chromene Schiff's bases **4a–d**.

different aromatic ketone and aldehydes such as; α-tetralone, isatin, 1-indanone, and 4-carboxybenzaldehyde in refluxing ethanol led to the formation of the corresponding target Schiff's bases **4a–d**. The molecular structures of the new compounds were confirmed *via* micro and spectral analyses. The FT-IR spectra of compounds **4a–d** showed absorption bands at 3355–3340 cm^{-1} related to the NH group, 1720–1710 cm^{-1} (lactonic –C=O carbonyl stretching), and 1671–1650 cm^{-1} (amide –C=O carbonyl stretching). The ^{1}H-NMR and ^{13}C-NMR spectral data of compounds **4a–d** confirmed the presence of these derivatives as trans and cis conformers in ratios ranging between 2 : 1 and 3 : 1. The ^{1}H-NMR and ^{13}C-NMR spectral data of compounds **4a–d** showed that they are present as trans and cis isomers. The ^{1}H-NMR spectra of compounds **4a–d** exhibited three singlets at δ 2.39–2.40, 4.84–5.45, and 6.21–6.25 ppm related to CH_3, O–CH_2, and coumarin-H_3, respectively. In addition, the methine proton of the N=CH group of compound **4d** appeared as a singlet signal at δ 8.07 and 8.38 ppm, while the NH proton appeared as an exchangeable signal at δ 10.62–13.70 ppm. The aromatic protons appeared as multiplet signals in the range δ 6.94–8.08 ppm. ^{13}C-NMR spectra of compounds **4a–d** showed signals at δ 18.53–18.55 and 65.70–66.54 ppm due to CH_3 and OCH_2 carbons alongside different signals at the range δ 101.97–160.40 ppm representing coumarin-C_3, N=CH, and the aromatic carbons. The carbonyl groups appeared as two singlets at δ 161.79 and 169.63 ppm. The mass spectra of the new compound **4a–d** represented their molecular ion peaks which were in agreement with their molecular formulae (Scheme 1).

3.2. *In vitro* studies

3.2.1. Acetyl cholinesterase inhibition and DPPH scavenging activity. The acetylcholinesterase inhibitory activity of the synthesized compounds **4a–d** was evaluated in comparison to the standard drug donepezil, and the results are shown in Table 1 as IC_{50} (μg mL^{-1}) values. The tested compounds showed IC_{50} values ranging from 0.802 to 7.869 μg mL^{-1} against AChE. The obtained data indicated that the indene analogue **4c** represented the most potent suppression activity that is close to that obtained by the reference drug donepezil, with IC_{50} values of 0.802 and 0.155 μg mL^{-1}, respectively. An observable decrease in activity was detected by the benzoic acid analogue **4d**, which produced an IC_{50} value of 1.20 μg mL^{-1}. This indicates that the increased lipophilic characteristic of the substituent at coumarin's position 7 is more favourable for its promising inhibitory potency. Furthermore, the increase in the size of the substituent, as in the case of tetralone analogue **4a**, reduced the inhibition potency with an IC_{50} value of 4.941 μM. A

Table 1 AChE inhibiting activity of the new compounds[a]

Compound no.	AChE IC_{50} (μg mL^{-1})	SD (±)
4a	4.941	0.25
4b	7.869	0.4
4c	0.802	0.04
4d	1.20	0.06
Donepezil	0.155	0.01

[a] Data are mean ± of three replicate in each group.

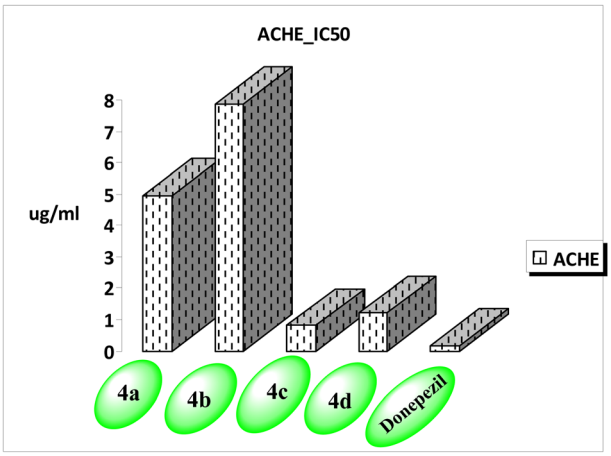

Fig. 3 AChE inhibiting activity of the new compounds.

Table 2 Percent of antioxidant activity of the new coumarin compounds[a]

Compounds	Concentration (0.01 mg)	Concentration (0.05 mg)
4a	31.8 ± 0.2	40.9 ± 3.1
4b	31.8 ± 1.2	35.00 ± 1.00
4c	28.00 ± 0.4	57.14 ± 2.77
4d	4.5 ± 0.4	10.3 ± 0.33
Vitamin C	80.00 ± 5.00	89.00 ± 6.99

[a] Data are means ± SD of three replicates in each group.

further reduction in potency was detected by the indole analogue **4b** with an IC_{50} value of 7.869 μM (Table 1 and Fig. 3).

In addition, the new compounds **4a–d** were subjected to DPPH scavenging assay to evaluate their antioxidant activity in comparison with vitamin C as a reference drug. Table 2 shows the percentage of free radical scavenging activity at two different concentrations of 0.01 mg, and 0.05 mg. The results showed that the activity of the tested analogues increased in a dose dependent manner. The most promising antioxidant activity was obtained by compound **4c** in comparison with vitamin C, with a DPPH percentage of inhibition 57.14 ± 2.77%, and 89.00 ± 6.99%, respectively, at 0.05 mg. Low inhibition activities were obtained by compounds **4a** and **4b** with percentages of 40.9 ± 3.1, and 35.00 ± 1.00%, respectively. Compound **4d** appeared to be inactive as an antioxidant agent, showing a percentage of inhibition 10.3 ± 0.33%.

Table 4 Hepatic enzyme levels in male rats after supplementation with 10 mg per kg body weight of the synthetic chemical compound **4c**

Groups	ALT (U/l)	AST (U/l)	ALP (U/l)
Control male rats	68.00 ± 3.00[a]	29.00 ± 2.00[a]	134.00 ± 8.00[a]
Treated male rats	79.00 ± 4.40[a]	32.00 ± 1.20[a]	136.00 ± 9.00[a]

[a] Data are means ± SD of 8 rats in the treated group. Statistical analysis was carried out using Co-state and SPSS computer programs (version 8), where the unshared letter is significant at $P \leq 0.05$.

Table 5 Levels of urea and creatinine in male rats after supplementation with 10 mg per kg body weight of the synthetic chemical compound **4c** [a]

Groups	Urea (mg dL^{-1})	Creatinine (mg dL^{-1})
Control male rats	18.60 ± 1.22	2.40 ± 0.10
Treated male rats	20.00 ± 1.57	2.80 ± 0.07

[a] Data are means ± SD of 15 rats in the treated group. Statistical analysis was carried out using co-state and SPSS computer programs (version 8), where the unshared letter is significant at $P \leq 0.05$.

3.2.2. Chronic toxicity, biochemical and hematological effects of compound 4c in rats. Due to the promising acetylcholinesterase inhibition activity of compound **4c**, it was of interest to study its safety profile on blood picture, hepatic enzymes, urea, and creatinine levels in a male rat group treated with supplementation of 10 mg per kg b.wt of **4c** for one month. The resultant data were compared with those obtained by the untreated control group. The results are summarized in Tables

Table 3 Blood profile in male rats after one month of supplementation with 10 mg per kg body weight of the synthetic chemical compound **4c**

Blood components	Control rats	**4c**-treated rats
Hemoglobin (Hb) (g L^{-1})	14.55 ± 0.14[a]	14.58 ± 0.59[a]
Red blood cells (RBCs) (million cells per mm)	7.88 ± 0.22[a]	8.00 ± 0.08[a]
Haematocrit (%)	45.90 ± 0.11[a]	45.00 ± 1.87[a]
Mean corpuscular volume (MCV) (fL)	55.50 ± 0.20[a]	59.00 ± 0.03[a]
Mean corpuscular hemoglobin (MCH) (pg)	17.00 ± 0.90[a]	17.78 ± 0.88[a]
Mean corpuscular hemoglobin concentration (MCHC) (g dL^{-1})	34.78 ± 0.29[a]	33.98 ± 0.25[a]
RDW-CV (%)	16.00 ± 0.60[a]	15.80 ± 0.19[a]
Platelets (10^3 mm^{-1})	449.00 ± 14.80[a]	465.00 ± 12.00[a]
MPV (fL)	7.19 ± 0.11[a]	8.66 ± 0.19[a]
White blood cells WBCs (10^3 cmm^{-1})	10.00 ± 0.10[a]	10.89 ± 1.90[a]
Neutrophils (10^3 cm^{-1})	2.59 ± 0.07[a]	2.39 ± 0.09[a]
Lymphocyte (10^3 cm^{-1})	7.88 ± 0.22[a]	7.62 ± 0.66[a]
Monocyte (10^3 cm^{-1})	1.87 ± 0.08[a]	1.93 ± 0.06[a]

[a] Data are means ± SD of 8 rats in the treated group. Statistical analysis was carried out using co-state and SPSS computer programs (version 8), where the unshared letter is significant at $P \leq 0.05$.

3–5. Table 3 showed insignificant changes in blood profile levels between the control and treated rats. Also, Table 4 exhibited an insignificant difference in the hepatic enzyme levels (AST, ALT, and ALP) as compared to the corresponding control group. Moreover, an insignificant change in the total urea level was detected in the **4c**-treated rats, while a significant increase in the creatinine level was detected in the **4c**-treated group when compared with the untreated one (Table 5).

3.2.3. Histopathological examination of chronic toxicity study. Light microscopic examination of hepatic tissue sections from normal control mice revealed the normal architecture of hepatic lobules, which consist of a central vein and hepatocytes arranged in hepatic cords around the central vein (Fig. 4a). Likewise, the liver of mice administered compound **4c** showed only slight Kupffer cell proliferation (Fig. 4b). Concerning kidneys, renal tissue from control mice revealed normal histological structure of glomeruli and renal tubules (Fig. 4c). Furthermore, kidney sections of mice administered compound **4c** exhibited histologically normal renal parenchyma with no histopathological alterations (Fig. 4d). In addition, the examined slices from all experimental groups (control and **4c**-treated) showed no histopathological damage in the heart and brain and appeared histologically normal (Fig. 4e–h).

3.2.4. Behavioural assessment of the effect of compound 4c in AD-induced rats. The T-maze test results demonstrated a significant increase in the time (seconds) taken by rats to reach the food in the T-maze for the $AlCl_3$-neurotoxicant rats (AD-group), denoting deteriorated neurocognitive function, with a percentage increase of 243.92% (Table 6). Whereas AD-groups treated with **4c** showed a significant decrease in the time taken by the rats to reach food compared to donepezil, with percentages of improvement reaching 148.37% compared

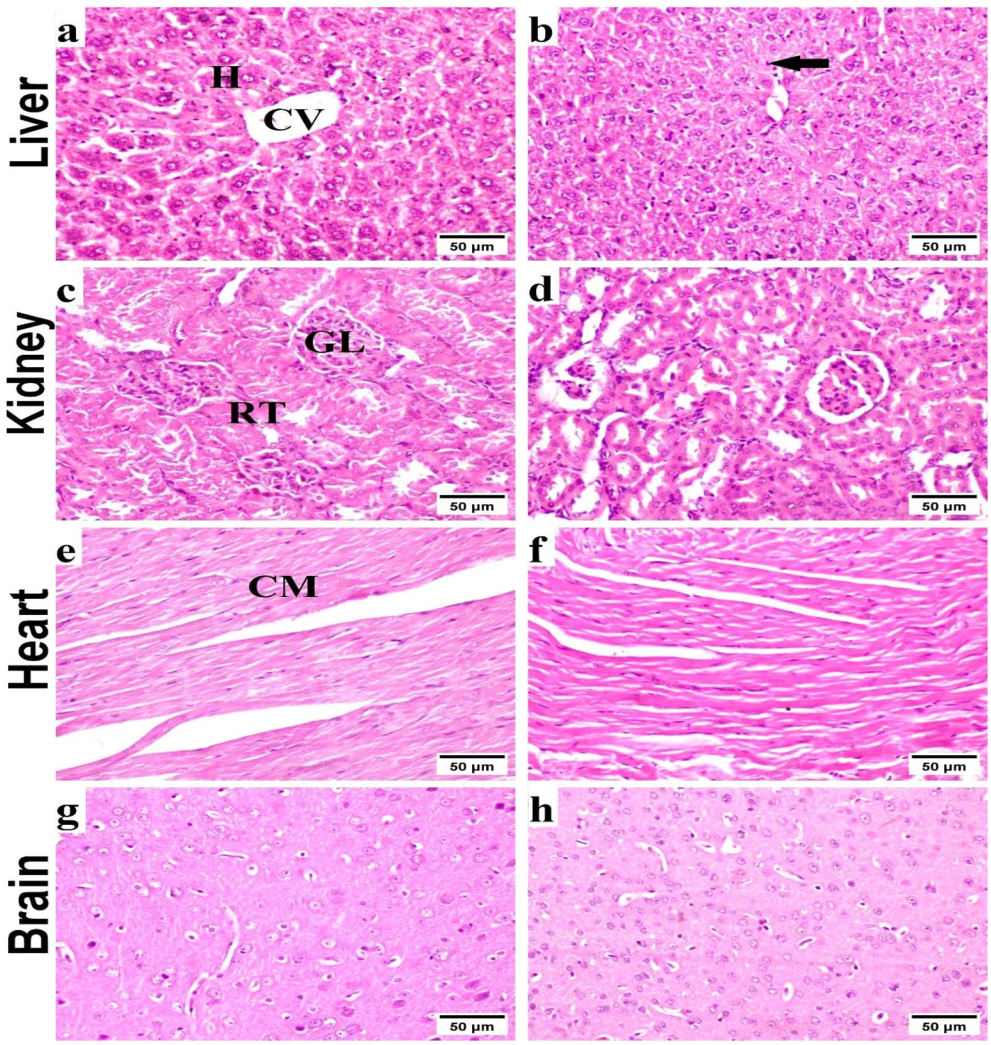

Fig. 4 Representative photomicrographs exhibited H & E-stained sections of liver (a and b), kidney (c and d), heart (e and f) and brain (g and h) respectively (scale bar, 50 μm); (a) normal control liver with normal hepatic tissue histoarchitecture: normal central vein (CV) and normal hepatocytes (H). (b) Received compound **4c**, showing slight Kupffer cell activation (arrow). (c) Normal control kidneys, showing the histological structure of renal parenchyma; normal glomeruli (GL), and renal tubules (RT). (d) Received compound **4c**, showing no histopathological alterations. (e) Normal control heart exhibiting normal cardiac myocytes. (f) Received compound **4c**, showing normal cardiac tissue. (g and h) Normal control brain extracts, showing histologically normal brain tissues with no histopathological alterations.

Table 6 Efficacy of compound **4c** in AD-induced rats using T-maze test[a]

Tested groups	Baseline (Sc)	Induction two months (Sc)	Treatment 4 weeks (Sc)
Control	13.30 ± 1.00	14.80 ± 1.00	14.90 ± 1.00
$AlCl_3$-AD	15.30 ± 1.10	50.90 ± 3.00	—
% change	1.53	243.92	
AD-**4c**	—	—	28.20 ± 1.80
% improvement			148.37
Donepezil	—	—	23.10 ± 1.70
% improvement			181.70

[a] Data are expressed as mean SD ($n = 10$) in seconds. Groups with similar letters are not significantly different, while those with different letters are significantly different at $p \leq 0.05$.

Table 7 Efficacy of compound **4c** on the beam balance test in Alzheimer's disease-induced rats

Tested groups	Baseline (Sc)	Induction 2 months (Sc)	Treatment 4 weeks (Sc)
Control	9.60 ± 0.87	9.80 ± 0.66	10.15 ± 0.22
$AlCl_3$-AD	9.00 ± 1.10	2.90 ± 0.70	—
% change	6.25	70.41	
AD-**4c**	—	—	8.99 ± 1.00
% improvement			60.00
Donepezil standard drug	—	—	9.80 ± 0.88
% improvement			67.98

to the standard drug (181.70%). The results of the beam balance test revealed that $AlCl_3$ caused a 70.41% decrease in the brain cognitive functions of $AlCl_3$-neurotoxicant rats (AD-group) (Table 7). However, treatment of rats with donepezil and the compound **4c** resulted in an improvement in their behavioural status, which was represented by improved motor coordination and improved cognition, with percentage improvements reaching 60.00%, compared to the standard drug (donepezil), which recorded 67.98%.

3.2.5. Effect of compound 4c on the antioxidant status of AD-induced rats. Examining the brain tissue of AD-induced rats compared to control rats brain cells, it has been found that there was a significant increase in MDA (181.54%) concomitant with a significant decrease in GSH (54.15%). Treatment of AD rats with the compound **4c** showed noticeable ameliorations in MDA and GSH, reaching 90.64 and 27.17%, respectively, compared to the standard drug, which recorded improvement percentages of 90.64% and 35.03% for MDA and GSH, respectively (Table 8).

3.2.6. Effect of compound 4c on *Bcl-2*, *Bax* and *Tau* gene. The present study also aimed to investigate the effect of the compound **4c** as on the expression of B-cell lymphoma-2 (*Bcl-2*), *Bcl-2*-associated X protein (*Bax*), and *tau* genes in $AlCl_3$-neurotoxicant rats (AD-group). The *Bcl-2* family is intricately involved in neuronal apoptosis; *Bcl-2* is an important endogenous anti-apoptotic gene, *Bax* is the most important pro-apoptotic gene in this family and the ratio between these two genes plays a role in the physiological state. Previous experiments have shown

Table 8 The effectiveness of compound **4c** in reducing oxidative stress in AD-induced rats[a]

Group/parameters	MDA (mg per g tissues)	GSH (mg per g tissues)
Control	11.75 ± 0.43	29.66 ± 0.55
AD	33.08 ± 2.10	13.60 ± 0.91
% change	181.54	54.15
4c-AD treated	22.43 ± 1.66	21.66 ± 1.21
% change to disease	32.19	59.26
% improvement	90.64	27.17
Donepezil-AD treated	22.43 ± 2.00	23.99 ± 2.00
% change to disease	32.19	76.40
% improvement	90.64	35.03

[a] Data are expressed in seconds as mean ± SD ($n = 8$). Groups with similar letters are not significantly different, while those with different letters are significantly different at $p \leq 0.05$.

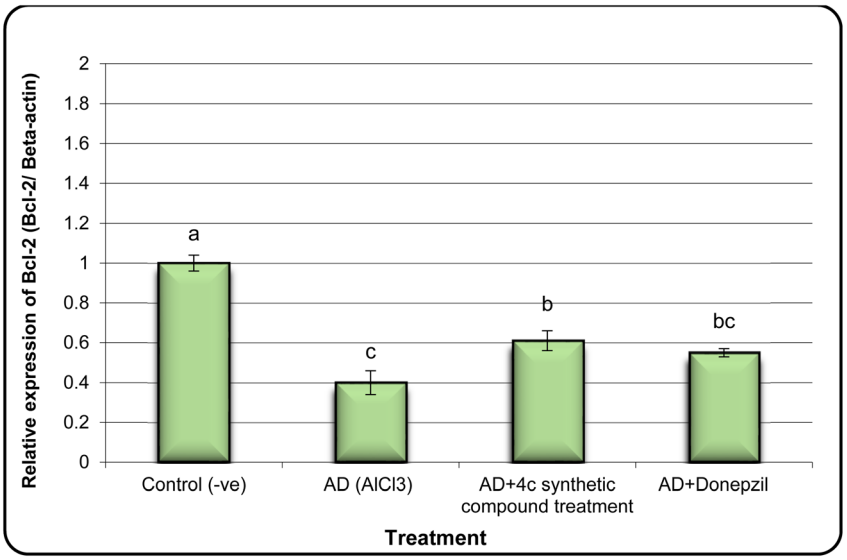

Fig. 5 The expression alterations of *Bcl-2* gene in brain samples of AD induced rats treated with compound **4c**. Means with different superscripts (a, b, c) between groups in the same treatment are significantly different at $P < 0.05$. Data are presented as mean ± SD.

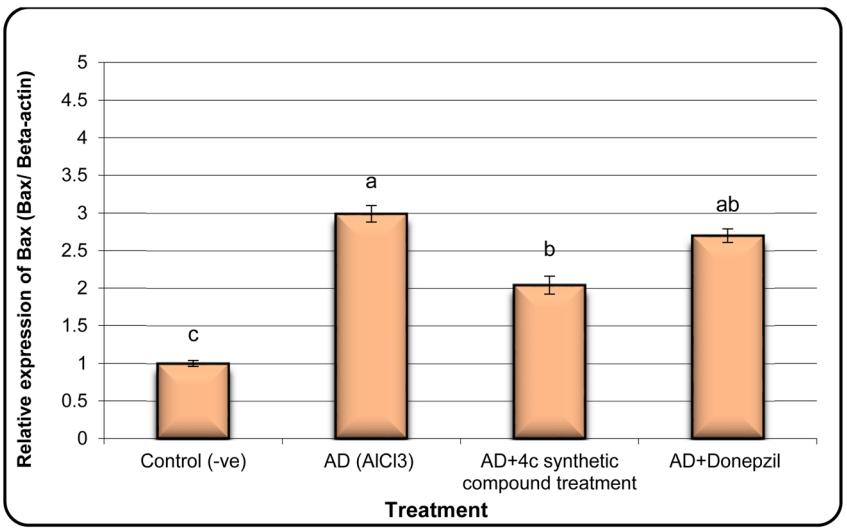

Fig. 6 The expression alterations of *Bax* gene in brain samples of AD induced rats treated with the compound **4c**. Means with different superscripts (a, b, c) between groups in the same treatment are significantly different at $P < 0.05$. Data are presented as mean ± SD.

that overexpression of tau genes can lead to increase toxicity in neural cells, reduced *Bcl-2* expression, increased *Bax* expression, and imbalanced *Bax*/*Bcl-2* ratios, all of which undermine the integrity of cell membranes.[36–40]

In the same line, we have found that AD rats exhibited down-regulation of *Bcl-2* expression and overexpression of the *Bax* and *Tau* genes. However, AD rats treated with compound **4c** showed improved expression of *Bcl-2* and reduced expression of *Bax* and *Tau* genes (Fig. 5–7).

3.3. Molecular docking studies

In order to validate our rational design, compounds **4a–4d** were docked against the acetylcholine esterase enzyme. The crystal structure of the acetylcholinesterase complex with donepezil (PDB: 1EVE) was used as a target for the molecular modelling analysis.[41,42] In order to validate the docking protocol, the native ligand (donepezil) was re-docked using MOE. The self-docking result showed that the RMSD value between the native ligand and the re-docked pose ≤2 Å which indicated the reliability of the docking protocol. The docking results of donepezil revealed interactions between the di-methoxy phenyl group and Trp279, while the phenyl group demonstrated an arene–arene interaction with Trp84. The N atom of the piperidine ring showed arene–cation interactions with Trp84 and Phe330. Hydrophobic interactions were found between donepezil and Leu282, Phe288 and Phe290, and Phe331. Tyr121 showed hydrophilic interactions with the carbonyl group (Fig. 8).

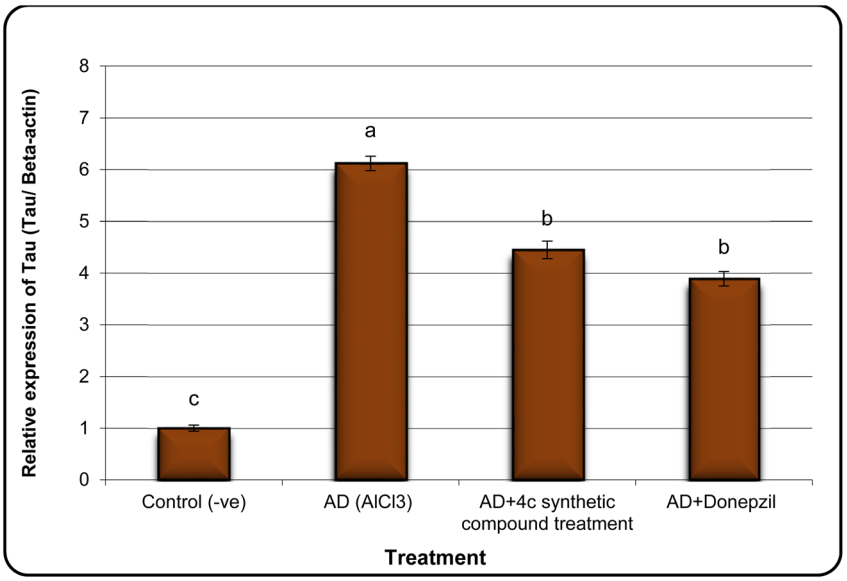

Fig. 7 The expression alterations of *Tau* gene in brain samples of AD induced rats treated with the compound **4c**. Means with different superscripts (a, b, c) between groups in the same treatment are significantly different at $P < 0.05$. Data are presented as mean ± SD.

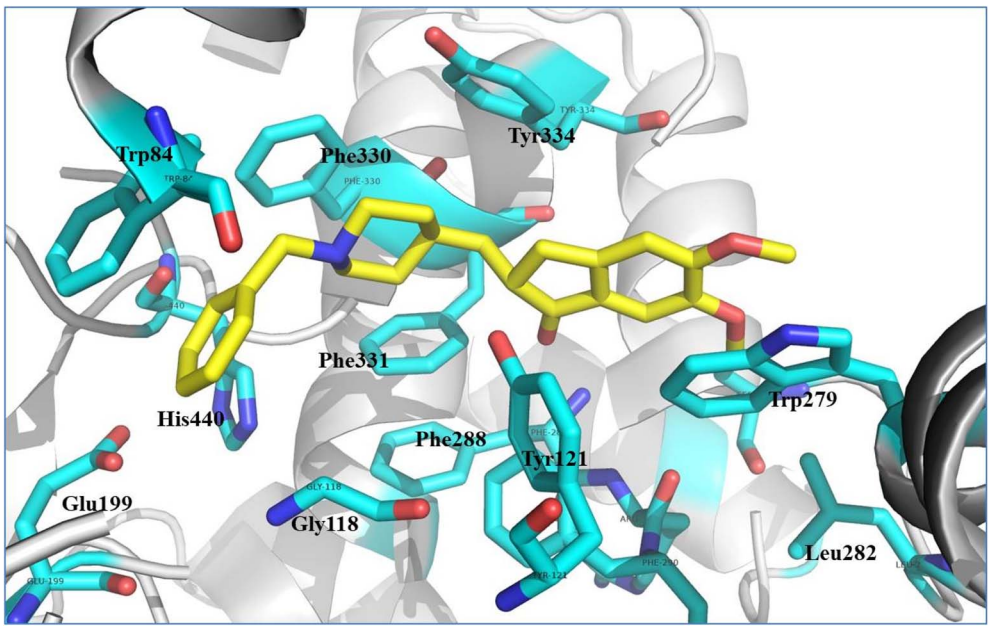

Fig. 8 Illustrated interaction of the native ligand (yellow stick) with amino acid residues (cyan stick), the protein is represented as a white cartoon.

We studied the binding mode and the interactions between the compounds **4a–4d** and the active site of the enzyme. Compounds **4a** and **4b** showed good binding modes within the active site in comparison with the native ligand (Fig. 9a and 10a, respectively). The two compounds nearly showed the same binding mode with binding scores of −8.7 and −7.4 kcal mol^{-1}, respectively (Table 9). Compound **4a** showed H-bonds with OH-Tyr121 and OH-Tyr130 at a distance (2.5 and 3.2 Å), respectively. The chromen and naphthalene moieties showed arene–arene (π–π) interactions with Trp84 and Trp279, respectively. The naphthalene moiety showed hydrophobic interactions with Phe331 and the hydrophobic part of Tyr334 (Fig. 9b). While compound **4b** showed a H-bond with OH-Tyr121 at a distance 3.1 Å, arene–arene interactions with Trp48 and Trp279. The chromen moiety showed hydrophobic interactions with Phe290, Phe331, and Tyr334 (Fig. 10b).

Compound **4c**, the most promising compound, showed the best docking score (−9.1 kcal mol^{-1}) and the best binding mode (Fig. 11a). Compound **4c** showed H-bonds between C=O of chromen and OH-Tyr130 at a distance of 2.5 Å and C=O of acetohydrazide and Tyr121 at a distance 2.9 Å (Fig. 11b). The chromen moiety showed arene–arene interactions with Trp84,

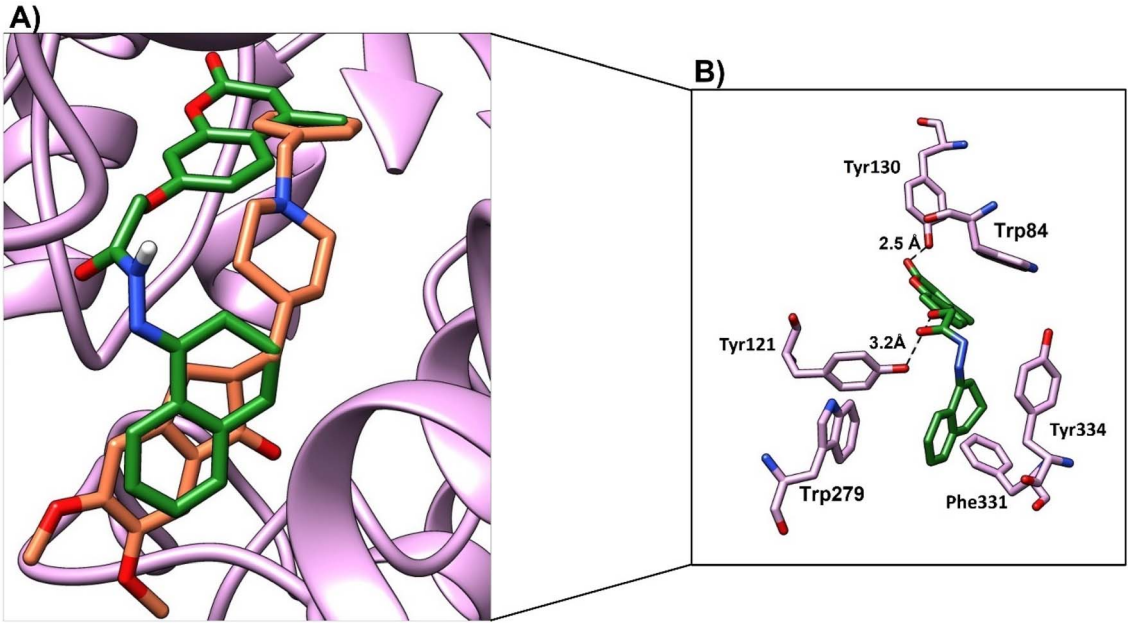

Fig. 9 (A) Binding mode of **4a** (green, stick) and native ligand (brown, stick) within the active site. (B) Interactions of compound **4a** (green) and key residues (purple), H-bond was represented as a black-dotted line.

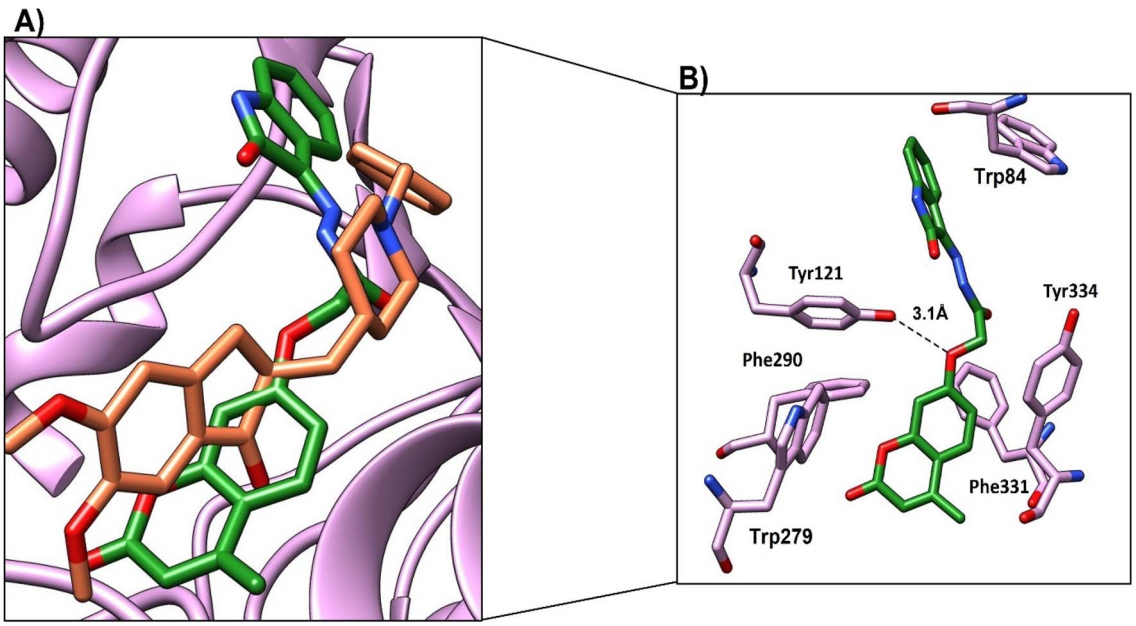

Fig. 10 (A) Binding mode of **4b** (green, stick) and native ligand (brown, stick) within the active site. (B) Interactions of compound **4b** (green) and the key residues (purple), H-bond was represented as a black-dotted line.

while the indene moiety showed arene–arene interactions with Trp279 and showed hydrophobic interactions with Phe330, Phe331 and Tyr 334 (Fig. 11b and Table 9).

Compound **4d** showed a moderate binding mode (binding score of -8.1 kcal mol^{-1}) as the chromen moiety moved a little away from the binding site (Fig. 12a). However, compound **4d** showed good interactions with the active site residue; the oxygen atom of 4-(methyl-2-oxo-2*H*-chromen-7-yl)oxy formed a H-bond with OH-Tyr121 at distance (3 Å), and C=O of benzoic acid formed a H-bond with Tyr130 at distance (2.2 Å) (Fig. 11b and Table 9). The chromen moiety showed arene–arene interactions with Trp279 and hydrophobic interactions with Phe330 and Phe 331.

In conclusion, the four compounds showed good binding modes and nearly similar poses within the active site of the cholinesterase enzyme. However, compound **4c** showed the best

Table 9 Results of molecular docking study of compounds **4a–4d** within the active site of acetylcholine esterase

Compd no.	Moieties from compounds	Residue-ID	Distance (Å)	Type of interactions	Score (kcal mol^{-1})
4a	(1) Oxygen atom of 4-methyl-2-oxo-2*H*-chromen-7-yl)oxy	OH-Tyr121	3.2	H-bond	−8.7
	(2) C═O of 4-methyl-2-oxo-2*H*-chromen moiety	OH-Tyr130	2.5	H-bond	
	(3) Chromen moiety	Trp84		π–π	
	(4) Naphthalene moiety	Trp279		π–π	
		Phe331, Tyr334		Hydrophobic	
4b	(1) Oxygen atom of 4-methyl-2-oxo-2*H*-chromen-7-yl)oxy	OH-Tyr121	3.1	H-bond	−7.4
		Trp279		π–π	
	(2) Chromen moiety	Phe290, Phe331, Tyr334		Hydrophobic	
	(3) Oxoindoline moiety	Trp84		π–π	
4c	(1) Carbonyl of 4-methyl-2-oxo-2*H*-chromen-7-aryloxy	OH-Tyr130	2.5	H-bond	−9.1
	(2) C═O of acetohydrazide	OH-Tyr121	2.9	H-bond	
	(3) Chromen moiety	Trp84		π–π	
	(4) Indene moiety	Phe330, Phe331, Tyr334		Hydrophobic	
		Trp279		π–π	
4d	(1) Oxygen atom of 4-methyl-2-oxo-2*H*-chromen-7-yl)oxy	OH-Tyr121	3.0	H-bond	−8.1
	(2) Chromen	Trp279		π–π	
	(3) C═O group of benzoic acid	Phe330, Phe331, Tyr334		Hydrophobic	
	(4) Phenyl group of benzoic acid	OH-Tyr130	2.2	H-bond	
		Trp84		π–π	

binding mode and the best binding score, which indicates the stability of the compounds within the acetylcholine esterase pocket. This result may explain the promising activity of **4c**. All compounds showed good interactions with Tyr121, Tyr130, and hydrophobic residues Phe330 and Phe 331. Besides, the arene–arene interactions with Trp84 and trp279.

3.3.1. Pharmacokinetics analyses. We studied the pharmacokinetic profile of lead compound **4c**. The compound contains a 7-alkoxy coumarin moiety, which undergoes metabolism using liver microsomes. The microsomal enzyme catalyzed the dealkylation of 7-alkoxy coumarin to 7-hydroxycoumarin in the presence of NADPH and molecular oxygen. In the presence of NADPH and oxygen, the metabolite 7-hydroxycoumarin is metabolized to unidentified metabolite(s) at a very slow rate. The formation of the conjugate of 7-hydroxycoumarin with glucuronic acid happens in the presence of UDPGA.[43]

The drug-likeness, Lipinski's, and ADM/Tox (absorption, distribution, metabolism, and toxicology) properties of

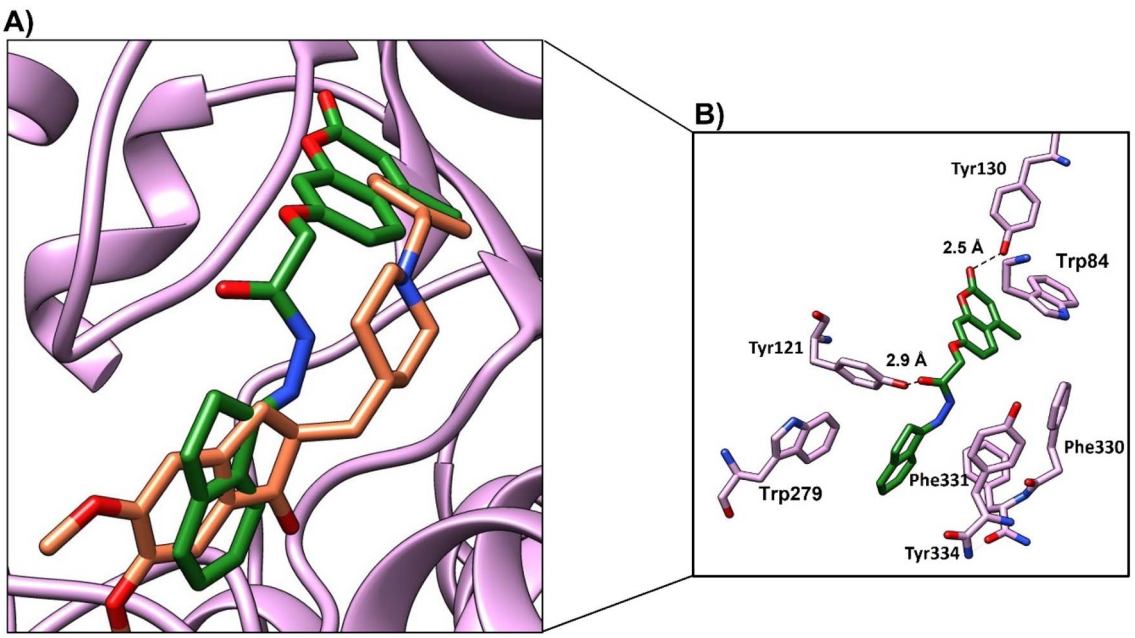

Fig. 11 (A) Binding mode of **4c** (green, stick) and native ligand (brown, stick) within the active site. (B) Interactions of compound **4c** (green) and the key residues (purple), H-bond represented as a black-dotted line.

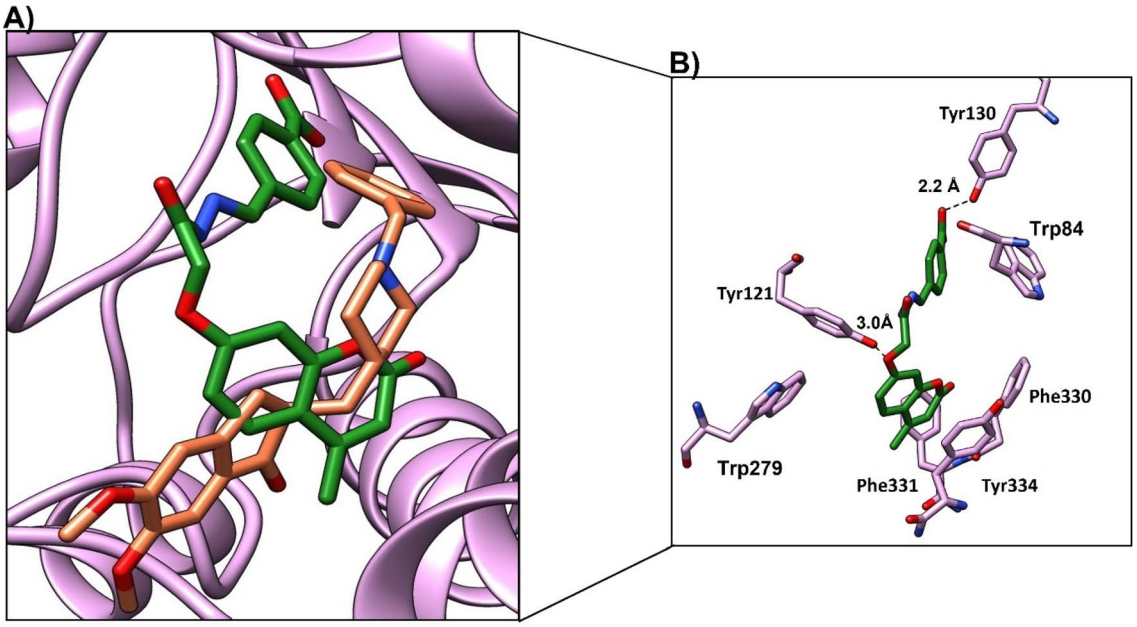

Fig. 12 (A) Binding mode of **4d** (green, stick) and native ligand (brown, stick) within the active site. (B) Interactions of compound **4d** (green) and key residues (purple), H-bond represented as a black-dotted line.

Table 10 Drug likeness properties and Lipinski's rule of compound **4c** [a]

Drug likeness parameters	Compound **8**
Smile	[O+]=1c2c(CC=1c1nn(cc1C1=C(C#N)C(=O)N(N)C(N)=C1C#N)-c1ccccc1)cccc2
MW	362.39
log $P_{o/w}$	2.95
HBD	1
HBA	5
NRB	4
MR	102.39
TPSA	80.90 Å^2
Lipinski	Yes (no violation)
Bioavailability score	3.54
PAINS filtrate	0 alert
Synthetic accessibility	3.54

[a] MW = molecular weight, log $P_{o/w}$ = lipophilicity, HBD = hydrogen bond donor, HBA = hydrogen bond acceptor, NRB = no. of rotatable bonds, MR = molecular refractivity, SA = synthetic accessibility (from 1 (very easy) to 10 (very difficult)) TPSA = topological polar surface area, good ≤140 Å^2.

compound **4c** were assessed using SwissADME, pkCSM,[44] and Data Warrior.

It was observed that compound **4c** followed Lipinski's rule (compound **4c** showed molecular $C\log p < 5$, molecular weight ≤500, H-bonds acceptor <10, and H-bonds donor <5) and showed total polar surface area = 80.90 Å^2 which was ≤140 Å^2. These results indicate **4c** has good oral bioavailability and absorbance. Also, compound **4c** passed the PAINS filter, and the synthetic accessibility of **4c** is 3.54, which means it is an easily synthesized compound (Table 10).

Table 11 summarized the absorption, distribution, metabolism, and excretion of compound **4c**. It was observed that compound **4c** has good human intestinal absorption (92.5%), moderate Caco-2 permeability (0.82 cm s^{-1}), and low skin permeability, which indicates that compound **4c** is not suitable for transdermal preparations.

Cytochrome P450 is an important detoxification enzyme in humans, many drugs are activated or inhibited by cytochrome P450. It was found that compound **4c** is a CYP1A2 and CYP2D6 inhibitor. At the same time, compound **4c** is predicted to be

Table 11 Predicted pharmacokinetic properties (absorption, distribution, metabolism, and excretion) of compound **4c** [a]

Absorption	
Model name	Predicted value
Water solubility	−3.823 mol L^{-1}
Human intestinal absorption (HIA)	92.5
Caco2 permeability	0.82 cm s^{-1}
Skin permeability	−2.69
Distribution	
BBB permeability	−0.21
CNS permeability	−2.18
Metabolism	
CYP1A2 inhibitor	Yes
CYP2D6 inhibitor	No
CYP3A4 substrate	Yes
Excretion	
Total clearance	0.87 mL min^{-1} kg^{-1}
Renal OCT2 substrate	No

[a] HIA = human intestinal absorption [0–20 (poor), 20–70 (moderate), 70–100 (well)], Caco2 = *In vitro* Caco2 cell permeability, SP = skin permeability, BBB = blood–brain barrier permeability.

Table 12 Predicted toxicity and reproductive effect by Data Warrior

Test	Carcinogenicity (mouse)
Mutagen	None
Tumorigenic	None
Irritant	None
Reproductive effect	High

deactivated by the CYP3A4 enzyme. The total clearance rate of compound **4c** is 0.87 mL min^{-1} kg^{-1}. Toxicity evaluation of compound **4c** showed it is not tumorigenic, or mutagenic, and it is not a skin irritant, which indicated it has a safe profile. Also, it has a high reproductive effect.

In conclusion, compound **4c** has good binding within the active site, which is considered the most stable binding mode among other compounds. Also, compound **4c** showed the lowest binding energy score. The pharmacokinetic profile showed that it followed Lipinski's rule and had a good total polar surface area value, which revealed its good oral bioavailability. The pharmacokinetic profile of compound **4c** showed its high human intestinal absorption. The CYP3A4 enzyme is responsible for the deactivation of compound **4c**. Table 12 showed that compound **4c** is not mutagenic, not tumorigenic, and not an irritant. Fortunately, it revealed a safe toxicity profile.

4. Conclusion

This study represents the design and synthetic pathway for the synthesis of new 2-oxo-coumarin-7-oxymethylene acetohydrazide derivatives **4a–d**. The chemical structures of the new analogues were confirmed *via* IR, ^{1}H-NMR, ^{13}C-NMR, and Mass spectra. The newly synthesized compounds were evaluated as acetylcholinesterase (AChE) inhibitors and antioxidant agents in comparison to donepezil and ascorbic acid, respectively, as reference drugs. Compound **4c** represented the most promising AChE inhibitory impact, with an IC_{50} value of 0.802 μM and DPPH scavenging activity of 57.14 ± 2.77%. Moreover, the biochemical and haematological studies showed that compound **4c** produced an insignificant change in the blood profile levels, the hepatic enzyme levels (AST, ALT, and ALP-1), and the total urea between the control and **4c**-treated rats. Furthermore, normal architecture of hepatic lobules and normal renal parenchyma, as well as no histopathological damage in the examined hepatic, kidney, heart, and brain tissues, were obtained by the histopathological studies in **4c**-treated rats. In addition, the T-maze test investigated that AD-groups treated with **4c** exhibited a remarkable reduction in the time taken by the rats to reach food in comparison to donepezil, with percentages of improvement reaching 148.37% compared to the standard drug (181.70%). Also, **4c** detectably ameliorated MDA and GSH, reaching 90.64 and 27.17%, respectively, in comparison to the standard drug, which recorded improvement percentages of 90.64% and 35.03% for MDA and GSH, respectively. Also, compound **4c** increased the expression of *Bcl-2* gene and down-regulated the expression *Bax* and *Tau* genes in the brain samples of AD-induced rats treated with compound **4c** in a similar manner to that obtained by the reference drug donepezil.

In silico studies showed that compound **4c** has a promising binding mode within the active site of acetylcholine esterase and is considered the most stable binding mode among other compounds **4a**, **4b**, and **4d**. Also, compound **4c** exhibited the lowest binding energy score. In addition, the pharmacokinetic profile showed that compound **4c** followed Lipinski's rule, revealing its good oral bioavailability, its high human intestinal absorption, and that the CYP3A4 enzyme is responsible for the deactivation of compound **4c**. Compound **4c** is not mutagenic, not tumorigenic, and not an irritant. Fortunately, it revealed a safe toxicity profile. Accordingly, the coumarin analogue **4c** could be considered a basic nucleus in the field of drug discovery for new multi-targeted directed ligands against Alzheimer.

Ethical statement

All animal procedures were performed in accordance with the Guidelines for Care and Use of Laboratory Animals of National Research Centre, Dokki, Giza, Egypt (NRC) and Experiments were approved by the Animal Ethics Committee of The Medical Research Ethics Committee (MREC) of NRC no. 19301.

Conflicts of interest

There are no conflicts to declare.

Acknowledgements

This work has been performed through the project “Molecular Simulation to Explore Therapeutic Efficacy of Novel Compounds for Prevention and Management of Alzheimer's Disease” funded by the Egyptian Academy of Scientific Research and Technology under an agreement programme between the academy and the Indian Academy of Science.

References

1 R. L. Frozza, V. Mychael, M. V. Lourenco and F. G. De Felice, *Front. Neurosci.*, 2018, **12**, 1–13.
2 E. Karran and B. De Strooper, *Nat. Rev. Drug Discovery*, 2022, **4**, 306–318.
3 R. J. O'brien and P. C. Wong, *Annu. Rev. Neurosci.*, 2011, **34**, 185–204.
4 B. P. Greenwood, V. Tolstikov, P. P. Narain, J. Chaufty, V. R. Akmaev, V. V. ishnudas, S. Gesta, E. J. Nestler, R. Sarangarajan, N. R. Narain and M. A. Kiebish, *Handbook of Biomarkers and Precision Medicine*, Chapman and Hall/CRC, 1st edn, 2019, 529–537.
5 Z. Breijyeh and R. Karaman, *Molecules*, 2020, **25**(24), 5789.
6 G. Weinstein and S. Seshadri, *Alzheimer's Res. Ther.*, 2014, **6**(1), 1–10.
7 M. Pandareesh, T. Anand and F. Khanum, *Neurochem. Res.*, 2016, **41**, 985–999.

8 N. George, B. Al Sabahi, M. AbuKhader, K. Al Balushi, M. J. Akhtar and S. A. Khan, *J. King Saud Univ., Sci.*, 2022, **34**(4), 101977.
9 S.-Y. Lee, Y.-J. Chiu, S.-M. Yang, C.-M. Chen, C.-C. Huang, G.-J. Lee-Chen, W. Lin and K.-H. Chang, *CNS Neurosci. Ther.*, 2018, **24**(12), 1286–1298.
10 A. Stefanachi, F. Leonetti, L. Pisani, M. Catto and A. Carotti, *Molecules*, 2018, **23**(2), 250.
11 F. Annunziata, C. Pinna, S. Dallavalle, L. Tamborini and A. Pinto, *Int. J. Mol. Sci.*, 2020, **21**(13), 4618.
12 G. Moya-Alvarado, O. Yañez, N. Morales, A. González-González, C. Areche, M. T. Núñez, A. Fierro and O. García-Beltrán, *Molecules*, 2021, **26**(9), 2430.
13 E. Jameel, T. Umar, J. Kumar and N. Hoda, *Chem. Biol. Drug Des.*, 2016, **87**(1), 21–38.
14 K. M. Amin, D. E. Rahman, H. A. Allam and H. H. El-Zoheiry, *Bioorg. Chem.*, 2021, **110**, 104792.
15 A. Rehman, S. Magsi, M. A. Abbasi, S. Rasool, A. Malik, G. Hussain, M. Ashraf and N. Khalid, *Pak. J. Pharm. Sci.*, 2014, **27**, 271–278.
16 S. Ghanei-Nasab, M. Khoobi, F. Hadizadeh, A. Marjani, A. Moradi, H. Nadri, S. Emami, A. Foroumadi and A. Shafiee, *Eur. J. Med. Chem.*, 2016, **121**, 40–46.
17 S. Hamulakova, L. Janovec, M. Hrabinova, K. Spilovska, J. Korabecny, P. Kristian, K. Kuca and J. Imrich, *J. Med. Chem.*, 2014, **57**(16), 7073–7084.
18 S. M. Bagheri, M. Khoobi, H. Nadri, A. Moradi, S. Emami, L. J. Baleh, F. Jafarpour, F. H. Moghadam, A. Foroumadi and A. Shafiee, *Chem. Biol. Drug Des.*, 2015, **86**(5), 1215–1220.
19 A. S. Alpan, S. Parlar, L. Carlino, A. H. Tarikogullari, V. Alptüzün and H. S. Güneş, Synthesis, biological activity and molecular modeling studies on 1*H*-benzimidazole derivatives as acetylcholinesterase inhibitors, *Bioorg. Med. Chem.*, 2013, **21**(17), 4928–4937.
20 Y. M. Syam, S. S. El-Karim, T. Nasr, S. A. Elseginy, M. M. Anwar, M. M. Kamel and H. F Ali, *Bioorg. Med. Chem.*, 2019, **19**(3), 250–269.
21 G. L. Ellman, D. K. Courtney, V. Andreas and R. M. Featherstone, *Biochem. Pharmacol.*, 1961, **7**, 88–95.
22 I. Gulcin, H. A. Alici and M. Cesur, *Chem. Pharm. Bull.*, 2005, **53**(3), 281–285.
23 S. Y. Desoukey, W. M. El Kady, A. A. Salama, E. G. Hagag, S. M. El-Shenawy and M. El-Shanawany, *Int. J. Pharmacogn. Phytochem. Res.*, 2016, **8**(7), 1121–1131.
24 J. D. Bancroft, *Bancroft's Theory and Practice of Histological Techniques E-Book*, ed. K. S. Suvarna, C. Layton and J. D. Bancroft, 2019.
25 S. Reitman and S. Frankel, *Am. J. Clin. Pathol.*, 1957, **28**(1), 56–63.
26 A. Belfield and D. Goldberg, *Enzyme*, 1971, **12**, 561–573.
27 H. Bartels, M. Böhmer and C. Heierli, *Clin. Chim. Acta*, 1972, **37**, 193–197.
28 J. K. Fawcett and J. E. A. Scott, *J. Clin. Pathol.*, 1960, **13**, 156–1591.
29 M. A. Thrall, D. C. Baker, and E. D Lassen, *Veterinary Hematology and Clinical Chemistry*, Lippin-cott Williams and Wilkins, Philadelphia, USA, 2004.
30 M. Kawahara, M. Kato-Negishi and K. Tanaka, *Metallomics*, 2017, **9**, 619–633.
31 R. M. J. Deacon and J. N. P. Rawlins, *Nat. Protoc.*, 2006, **1**(1), 7–12.
32 E. Y. Pioli, B. N. Gaskill, G. Gilmour, M. D. Tricklebank, S. L. Dix, D. Bannerman and J. P. Garner, *Brain Res.*, 2014, **261**, 249–257.
33 M. Altun, E. Bergman, E. Edström, H. Johnson and B. Ulfhake, *Physiol. Behav.*, 2007, **92**(5), 911–923.
34 E. Beutler, O. Duron and B. M. Kelly, *Clin. Med.*, 1963, **61**, 882–888.
35 H. Ohkawa, N. Ohishi and K. Yagi, *Anal. Biochem.*, 1979, **95**, 351–358.
36 M. Callens, N. Kraskovskaya, K. Derevtsova, W. Annaert, G. Bultynck, I. Bezprozvanny and T. Vervliet, *Biochim. Biophys. Acta, Mol. Cell Res.*, 2021, **1868**(6), 118997.
37 H. Borai, M. K. Ezz, M. Z. Rizk, H. F. Aly, M. El-Sherbiny, A. A. Matloub and G. I. Fouad, *Biomed. Pharmacother.*, 2017, **93**, 837–851.
38 A. H. Elmaidomy, U. R. Abdelmohsen, F. Alsenani, H. F. Aly, S. G. E Shams, E. A. Younis, K. A. Ahmed, A. M. Sayed, A. I. Owis, N. Afifi and D. El Amir, *RSC Adv.*, 2022, **12**, 11769–11785.
39 H. Aly, N. Elrigal, S. Ali, M. Rizk and N. Ebrahim, *J. Mater. Environ. Sci.*, 2018, **9**, 1931–1941.
40 M. Z. Rizk, I. H. Borai, M. K. Ezz, M. El-Sherbiny, H. F. Aly, A. Matloub and G. I. Fouad, *J. Mater. Environ. Sci.*, 2018, **9**(7), 2098–2108.
41 S. A. Elseginy and M. M. Anwar, *ACS Omega*, 2021, **7**(1), 150–1164.
42 S. A. Elseginy, *J. Biomol. Struct. Dyn.*, 2022, **40**(24), 13658–13674.
43 T. Matsubara, E. Yoshihara, T. Iwata, Y. Tochino and Y. Hachino, Biotransformation of coumarin derivatives (1) 7-alkoxycoumarin O-dealkylase in liver microsomes, *Jpn. J. Clin. Pharmacol. Ther.*, 1982, **32**(1), 9–21.
44 D. E. Pires, T. L. Blundell and D. B. Ascher, pkCSM: predicting small-molecule pharmacokinetic and toxicity properties using graph-based signatures, *J. Med. Chem.*, 2015, **58**(9), 4066–4072.